

Coupling of a Single Diamond Nanocrystal to a Whispering-Gallery Microcavity: Photon Transportation Benefitting from Rayleigh Scattering

Yong-Chun Liu, Yun-Feng Xiao*, Bei-Bei Li, Xue-Feng Jiang, Yan Li, and Qihuang Gong†

State Key Lab for Mesoscopic Physics, School of Physics, Peking University, P. R. China.

We study the Rayleigh scattering induced by a diamond nanocrystal in a whispering-gallery-microcavity-waveguide coupling system, and find that it plays a significant role in the photon transportation. On one hand, this study provides a new insight into future solid-state cavity quantum electrodynamics toward strong coupling physics. On the other hand, benefitting from this Rayleigh scattering, novel photon transportation such as dipole induced transparency and strong photon antibunching can occur simultaneously. As potential applications, this system can function as high-efficiency photon turnstiles. In contrast to [B. Dayan *et al.*, *Science* **319**,1062 (2008)], the photon turnstiles proposed here are highly immune to nanocrystal's azimuthal position.

PACS numbers: 78.35.+c, 42.50.Pq, 42.50.Ar

Cavity quantum electrodynamics (CQED) studies light-matter interactions inside a resonator, which offers an ideal platform for quantum optics [1]. Tremendous progress has been made by coupling single dipoles to different microcavities (for a review, see [2]). Among them, whispering-gallery mode (WGM)-type microcavity [3] is most promising due to its extremely high Q factor, small mode volume, excellent scalability and ease for low-loss transport of nonclassical states using an optical fiber [4, 5]. On the other hand, nitrogen-vacancy (NV) centers have recently emerged as an important candidate for quantum information processing because they possess long-lived spin triplets at room temperature [6, 7]. Combining high-Q WGM microcavities and NV centers represents a promising solid-state CQED system, and attracts much attention very recently [4, 5, 8].

One of the distinct properties of WGMs is that they belong to traveling waves, unlike standing modes in a Fabre-Perot cavity. In other words, WGM microcavities typically support twin modes, clockwise (cw) and counter-clockwise (ccw) propagating waves with a degenerate frequency. In this paper, we investigate the interaction of the twin WGMs coupled to a NV center in a diamond nanocrystal. On one hand, we find that not only the dipole transition of the NV center but also the Rayleigh scattering by the nanocrystal itself play significant roles in the coupled system. Thus strong coupling condition in such CQED system should be re-defined. On the other hand, nonclassical effects are predicted benefitting from the nanocrystal scattering. Dipole induced transparency (DIT) [9] appears in the presence of the strong Rayleigh scattering, accompanying strong photon antibunching in transmitted fields. Moreover, high-efficiency photon turnstiles can be implemented highly

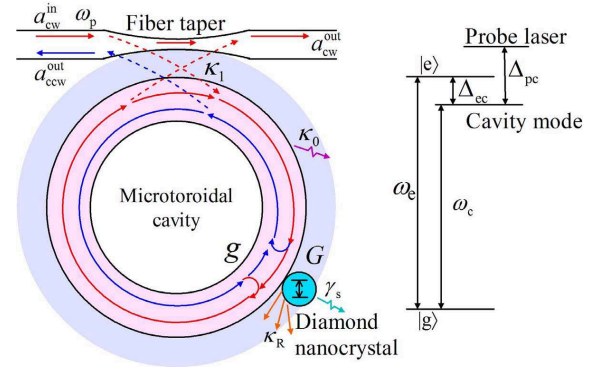


FIG. 1: Schematic illustration of the nanocrystal-microcavity-waveguide coupling system.

immune to the azimuthal position of the nanocrystal.

Figure 1 describes the present coupling system. A diamond nanocrystal embodying a single NV center is located on the surface of a microtoroidal cavity [10]. A tapered fiber is used to couple light with frequency ω_p in and out of the microcavity. Under the rotating wave approximation, the Hamiltonian of the coupled system can be written as ($\hbar = 1$)

$$\begin{aligned}
 H &= H_0 + H_1 + H_2, \\
 H_0 &= \omega_e |e\rangle \langle e| + \sum_m \omega_c a_m^\dagger a_m + \sum_{k=1}^3 \sum_j \omega_{kj} b_{kj}^\dagger b_{kj}, \\
 H_1 &= \sum_m G_m a_m^\dagger \sigma_- + \sum_j G_j b_{1j}^\dagger \sigma_- + H.c., \\
 H_2 &= \sum_{m,m'} g_{m,m'} a_m^\dagger a_{m'} + \sum_j (g_{cw,j} a_{cw}^\dagger b_{2j} + H.c.) \\
 &\quad + \sum_j (g_{ccw,j} a_{ccw}^\dagger b_{3j} + H.c.). \tag{1}
 \end{aligned}$$

Here summation indices (m, m') run through cw, ccw; a_m

*Author to whom correspondence should be addressed. Email: yfxiao@pku.edu.cn; URL: <http://www.phy.pku.edu.cn/~yfxiao/index.html>

†Email: qhgong@pku.edu.cn

and b_{kj} ($k = 1, 2, 3$) denote annihilation operators of the cavity and the reservoir modes, respectively; $\sigma_- = |g\rangle\langle e|$ and $\sigma_+ = |e\rangle\langle g|$ stand for the descending and ascending operators of the dipole transition at zero-phonon line. The Hamiltonian H_0 describes the free evolution of the system consisting of the NV center, WGMs and reservoir modes, with frequency ω_e , ω_c , ω_{kj} , respectively. The first (second) term in H_1 characterizes the dipole interactions between the NV center and WGMs (reservoir modes), with the coupling strength G_m (G_j). The first term in H_2 describes the nanocrystal-induced scattering into the same ($m = m'$) or the counter-propagating ($m \neq m'$) WGM fields with strengths $g_{m,m'}$, while the second term represents the WGMs-reservoir scattering coefficients $g_{m,j}$.

In the full quantum theory, the coherent coupling strengths G_m and G_j can be calculated by $G_m \equiv G = \mu(\omega_c/(2\hbar\varepsilon_0\varepsilon_s V_c))^{1/2} f_c(\vec{r})$ and $G_j = \mu(\omega_{1j}/(2\hbar\varepsilon_0\varepsilon_s V_{1j}))^{1/2}$, where $\mu = 2.74 \times 10^{-29}$ C·m represents the dipole moment of the NV center transition. ε_0 is the electric permittivity of the vacuum and $\varepsilon_s = 1$ denotes the relative permittivity of the surrounding medium (vacuum here). V_c and V_{1j} are the quantized volumes of the cavity and the reservoir modes interacting with the dipole, respectively. $f_c(\vec{r}) = |E(\vec{r})/E_{\max}|$ is the normalized field distribution function of WGMs. For the subwavelength nanocrystal, the above scattering interaction can be modeled in a dipole approximation where the electric field of the input wave (either WGMs or reservoir modes) induces a dipole moment in the scatterer, namely, *scattering induced dipole*. In the case of elastic Rayleigh scattering, the coupling strengths are $g_{m,m'} \equiv -g = -\alpha f_c^2(\vec{r})\omega_c/(2V_c)$ and $g_{m,j} \equiv -g_R = -\alpha f_c(\vec{r})\omega_c(\hat{n}_m \cdot \hat{n}_{k,j})/(4V_c V_{k,j})^{1/2}$ ($m = \text{cw}, k = 2$ or $m = \text{cw}, k = 2$) [11]. Here $\alpha = 4\pi R^3(\varepsilon_d - \varepsilon_s)/(\varepsilon_d + 2\varepsilon_s)$ is the polarizability for the spherical nanocrystal with radius R where $\varepsilon_d = 2.4^2$ denotes the electric permittivity of the diamond. \hat{n}_m and $\hat{n}_{k,j}$ are unit vectors of the fields.

We can find that both the NV center-reservoir and WGM-reservoir coupling interactions have the same format. By using Weisskopf-Wigner approximation, the coupling of the NV center to the reservoir can be regarded as a decay of the excited state, i.e., the well-known spontaneous emission with rate γ_s ; while the scattering of WGMs to the reservoir can be modeled by an energy damping of WGMs, with the damping rate $\kappa_R = \alpha^2 f_c^2(\vec{r})\varepsilon_s^{3/2}\omega_c^4/(6\pi c^3 V_c)$ [11], where c is the speed of light in vacuum. Transforming travelling to standing modes, $a_{\pm} = (a_{\text{cw}} \pm a_{\text{ccw}})/\sqrt{2}$, the equations of motion

for the coupled system are given by [12]

$$\frac{da_+}{dt} = (2ig - \kappa_+)a_+ - \sqrt{2}iG\sigma_- - \sqrt{\frac{\kappa_1}{2}}a_{\text{cw}}^{\text{in}} + \hat{\mathbf{f}}_+, \quad (2)$$

$$\frac{da_-}{dt} = -\kappa_-a_- - \sqrt{\frac{\kappa_1}{2}}a_{\text{cw}}^{\text{in}} + \hat{\mathbf{f}}_-, \quad (3)$$

$$\frac{d\sigma_-}{dt} = -(i\Delta_{\text{ec}} + \frac{\gamma_s}{2})\sigma_- + i\sqrt{2}Ga_+\sigma_z + \hat{\mathbf{f}}_1. \quad (4)$$

Here $\sigma_z \equiv |e\rangle\langle e| - |g\rangle\langle g|$, $\Delta_{\text{ec}} \equiv \omega_e - \omega_c$, $\kappa_+ = \kappa_R + (\kappa_0 + \kappa_1)/2$, $\kappa_- = (\kappa_0 + \kappa_1)/2$; $\kappa_0 = \omega_c/Q_0$ denotes the intrinsic damping of the WGMs with Q_0 being the intrinsic quality factor; κ_1 stands for the cavity-taper coupling strength; $a_{\text{cw}}^{\text{in}}$ is the input field. The operators $\hat{\mathbf{f}}_+$, $\hat{\mathbf{f}}_-$, $\hat{\mathbf{f}}_1$ are the noise operators that conserve the commutation relations at all times. One can find that the symmetric mode a_+ is strongly coupled to the NV center (through dipole interaction) and the nanocrystal (through the scattering), while the anti-symmetric mode a_- keeps uncoupled to them.

When the cavity is excited by a weak monochromatic field (i.e., weak-field approximation), the NV center is predominantly in the ground state. Thus σ_z can be substituted for its average value of -1 , and Eq. (4) becomes linear. Utilizing the standard input-output formalism $a_m^{\text{out}} = a_m^{\text{in}} + \sqrt{\kappa_1}a_m$ [12], we obtain the outputs

$$a_{\text{cw}}^{\text{out}} = \left[1 + \frac{\kappa_1}{2} \left(\frac{1}{D_+} + \frac{1}{D_-}\right)\right] a_{\text{cw}}^{\text{in}} + \hat{\mathbf{f}}'_2, \quad (5)$$

$$a_{\text{ccw}}^{\text{out}} = \frac{\kappa_1}{2} \left(\frac{1}{D_+} - \frac{1}{D_-}\right) a_{\text{cw}}^{\text{in}} + \hat{\mathbf{f}}'_3, \quad (6)$$

where $D_+ = i(\Delta_{\text{pc}} + 2g) - \kappa_+ + 2G^2/[i(\Delta_{\text{pc}} - \Delta_{\text{ec}}) - \gamma_s/2]$, $D_- = i\Delta_{\text{pc}} - \kappa_-$, with $\Delta_{\text{pc}} \equiv \omega_p - \omega_c$, $\hat{\mathbf{f}}'_2$ and $\hat{\mathbf{f}}'_3$ are noise operators. We take the cold reservoir limit where the reservoir modes are all initially in vacuum states. Thus the expectation values of all noise operators can be neglected because they are annihilated when acting on the initial vacuum states. Then the transmission $\langle a_{\text{cw}}^{\text{out}\dagger} a_{\text{cw}}^{\text{out}} \rangle / \langle a_{\text{cw}}^{\text{in}\dagger} a_{\text{cw}}^{\text{in}} \rangle$ and reflection $\langle a_{\text{ccw}}^{\text{out}\dagger} a_{\text{ccw}}^{\text{out}} \rangle / \langle a_{\text{cw}}^{\text{in}\dagger} a_{\text{cw}}^{\text{in}} \rangle$ can be determined.

Under practical parameters $\gamma_s/2\pi = 13$ MHz, $Q_0 = 10^8$, $\kappa_1 = 0.5\kappa_0$, $V_c \sim 200 \mu\text{m}^3$, $f_c(\vec{r}) \sim 0.47$, we obtain $\{G, \kappa_0, \kappa_1\}/2\pi \sim \{180, 4.7, 2.35\}$ MHz. We will use these parameters unless otherwise specified. Figure 2(a) plots these parameters depending on the particle radius R . We can approximately divide Fig. 2(a) into three regions. In region I, G far exceeds any other parameters for a small diamond nanocrystal. The NV center couples to the twin WGMs, creating a pair of standing modes. There exist three separate resonance dips in transmission spectrum: one at the original zero detuning due to the decoupling between the anti-symmetric mode and the NV center, and the other two splitted by $2\sqrt{2}G$ due to the strong coupling between the symmetric standing mode and the NV center. The linewidth of the central dip is $\kappa_0 + \kappa_1$; while the linewidths of the two sideward dips are

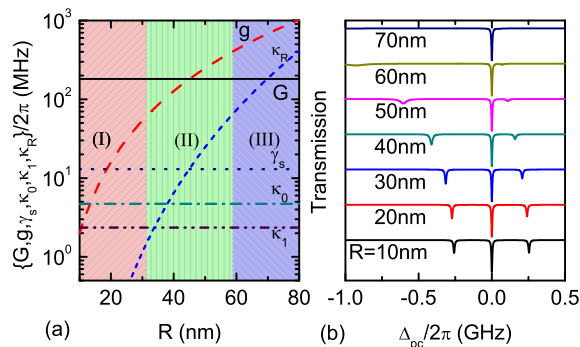


FIG. 2: (a) Parameters $\{G, g, \gamma_s, \kappa_0, \kappa_1, \kappa_R\}$ vs. the radius R of the nanocrystal. (b) The transmission spectra for various R . Here $Q_0 = 10^8$, $\kappa_1 = 0.5\kappa_0$ and $\Delta_{ec} = 0$.

$\kappa_R + (\kappa_0 + \kappa_1 + \gamma_s)/2$, which can be interpreted by the dressed state generated by the strong coupling.

With the increase of R , the coefficient g grows rapidly. In region II, g becomes comparable with G , while κ_R is still much smaller than G because $g(\kappa_R) \propto R^3(R^6)$. The scattering not only moves the two sideward resonances with detunings $-g \pm (g^2 + 2G^2)^{1/2}$, but also increases their linewidths and decreases the coupling efficiencies. When the size of the nanocrystal is large enough (region III), the scattering damping rate κ_R becomes comparable to or even exceeds G . In this situation, the scattering damping rate is so large that the two sideward dips nearly vanish. In all cases, the central dip keeps unchanged, and its coupling depends mainly on κ_0 and κ_1 .

Transmission spectra for different R varying from 10 to 70 nm are plotted in Fig. 2(b), confirming the above analysis. As the nanocrystal-induced scattering does occur, the new strong coupling condition requires that $G \gg \{\kappa_+, \gamma_s\}$, corresponding to regions I and II. This provides new insights into future solid-state CQED.

In the region where the present strong coupling condition does not match, interesting DIT effects in the transmission spectrum can be predicted. Let us consider the conditions for a general DIT phenomenon. First, in the absence of the dipole, the new critical coupling condition ($\kappa_1^2 = \kappa_0^2 + 4g^2$) is required to create a relatively broad platform with a low transmission. This can be implemented though the destructive interference among the directly transmitted field uncoupled to the microcavity and the output field via cavity modes, as discussed in detail in the following. Second, the linewidth of the resonance should be larger than the dipole-cavity coupling strength ($\kappa_+, \kappa_- > G$, *i.e.*, the bad cavity limit). These conditions are verified in Fig. 3, which presents the transmission, reflection and energy loss in different conditions.

In the weak scattering case ($g \ll \kappa_0$), the initial critical coupling condition without dipole is simplified as $\kappa_1 = \kappa_0$. For cavities with high intrinsic quality factor, the mode splitting occurs instead of DIT, as shown

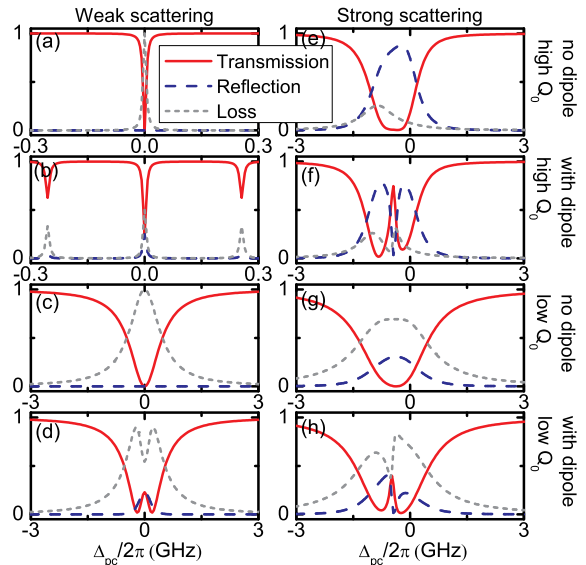


FIG. 3: Transmission, reflection and energy loss of the present system working on the critical coupling point $\kappa_1 = (\kappa_0^2 + 4g^2)^{1/2}$. (a)-(d), weak scattering case with $R = 6$ nm and $\Delta_{ec} = 0$. (e)-(h), strong scattering case with $R = 60$ nm and $\Delta_{ec} = -g - G^2/g$. The high and low Q_0 are 10^8 and 10^6 , respectively.

in Figs. 3(a)-3(b). This is because the dipole-cavity coupling strength exceeds the resonance linewidth. While a cavity with low intrinsic quality factor can produce DIT as shown in Figs. 3(c)-3(d), but there are significant energy losses, yielding the low DIT peak, as well as low on/off contrast ratio.

In the strong scattering case ($g \gg \kappa_0$), however, we find that the nanocrystal-induced Rayleigh scattering plays a constructive role in generating DIT and can significantly enhance it, as demonstrated in Figs. 3(e)-3(h). In general, the field radiated by the NV center dipole takes part in the interference mentioned above. If we control the detuning $\Delta_{ec} = -g - G^2/g$ so that the radiated field intensity has a maximum value at $\Delta_{pc} \simeq -g$ where the initial critical-coupling point is located at. The DIT window (also at $\Delta_{pc} \simeq -g$) with a high efficiency (the peak value exceeds 0.8) appears, because the intrinsic loss is far smaller than the cavity-taper coupling rate ($\kappa_1 \sim 2g \gg \kappa_0$).

High-efficiency DIT holds great potential for photon turnstiles [13, 14]. We are thus interested in the photon statistics of the output [15, 16], described by the second-order correlation functions $g_m^{(2)} = \langle (a_m^{\text{out}\dagger})^2 (a_m^{\text{out}})^2 \rangle / \langle a_m^{\text{out}\dagger} a_m^{\text{out}} \rangle^2$. Figure 4(a) depicts the strong photon antibunching of the transmitted field with a large bandwidth, corresponding to the case in Fig. 3(f). This is because the net transmitted field mainly originates from the NV center dipole and a single dipole cannot emit two or more photons simultaneously. Actually, excitation of the system by a first photon blocks

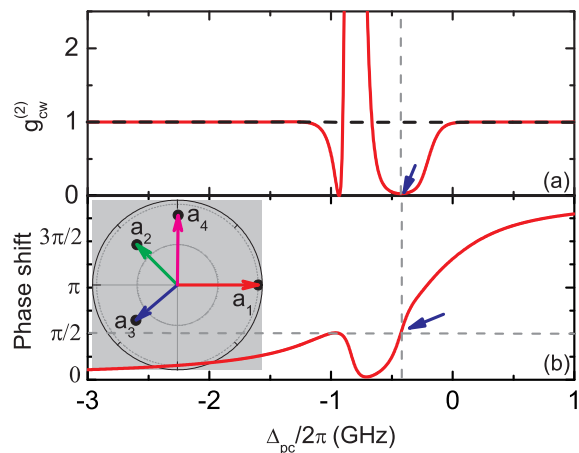


FIG. 4: Normalized second-order autocorrelation functions $g_{cw}^{(2)}$ (a) and phase shift (b) of the corresponding transmitted field in Fig. 3(f). The dashed vertical lines and blue arrows indicate the position of $\Delta_{pc} = -g$. Inset: Four components of the transmitted field in complex plane (see text).

the transmission of a second photon, known as photon blockade [17]. It is of importance that the strong antibunching ($g_{cw}^{(2)} = 0$) occurs exactly at the DIT window, which guarantees the high efficiency of the antibunched light.

In the DIT window, the phase shift ϕ_{cw} of the transmitted field (defined as $\phi_{cw} \equiv \arg[a_{cw}^{out}/a_{cw}^{in}]$) has also been plotted in Fig. 4(b), which exhibits a very large dispersion in the region near $\Delta_{pc} = -g$. This enables us to control the phase shift and group delay of the output field. It is interesting that the transmitted field experiences a $\pi/2$ phase shift at the DIT peak, different from the previous DIT in [9] (zero shift). To explicitly explain this, from Eq. (5), we note that the transmitted field is an interference of four components: directly transmitted field uncoupled to the microcavity, output field via the anti-symmetric mode, output field via the Rayleigh scattering, and output field via the NV-center dipole interaction, denoted by $a_{k=1,2,3,4}$, respectively. In the inset of Fig. 4(b) we plot the four components for $\Delta_{pc} = -g$ in the complex plane. Here, we find $a_1 = a_{cw}^{in}$ and $a_2 = (\kappa_1/2)a_{cw}^{in}/(i\Delta_{pc} - \kappa_-)$, which cannot be tuned via the nanocrystal; $a_3 = (\kappa_1/2)a_{cw}^{in}/(i(\Delta_{pc} + 2g) - \kappa_+)$ depends on the scattering strength g while a_4 depends

mainly on G and Δ_{ec} . It can be seen that a_1, a_2, a_3 destructively interfere, creating zero net field. a_4 has a large amplitude with the relative phase $\pi/2$. This further explains the strong antibunching of the transmitted field in the DIT window.

Finally, in Ref. [13], photon turnstiles are realized by coupling microcavity to single cooled caesium atoms. Standing wave modes built there are induced by scattering from defects and surface roughness of the microtoroidal cavity, and thus photon turnstiles are sensitive to the atom's azimuthal position. Averaging over the azimuthal angle results in a significant reduction of the on/off contrast ratio of transmission in the DIT window (see Fig. 1(E) in Ref. [13]). While in the present paper, Rayleigh scattering is induced by the diamond nanocrystal itself. Thus these devices are highly immune to azimuthal position of the nanocrystal. This is of special importance when multi-nanocrystal are involved in the microcavity system. For example, the dynamics of the coupling system will strongly depend on the inter-positions of these nanocrystals.

In summary, we have analyzed a single diamond nanocrystal with a NV center coupled to high-Q counter-propagating twin WGMs of a microtoroidal cavity. It is found that the Rayleigh scattering induced by the nanocrystal itself not only induces strong interaction between the twin WGMs, but also results in the scattering loss of the WGMs. This provides a new insight into future solid-state CQED. We also reveal that Rayleigh scattering can play a positive role in obtaining DIT with high efficiency, accompanying strong photon antibunching. The system can perform as photon turnstiles which are highly immune to the azimuthal position of nanocrystal. Our investigation can be of practical use in controlled interactions of single quanta and scalable quantum logic.

Note added - We note a recent publication [18] after the submission of our work.

Acknowledgments

This work was supported by NSFC (Nos. 10821062 and 11004003) and 973 program (No. 2007CB307001). Yun-Feng Xiao was also supported by the Research Fund for the Doctoral Program of Higher Education (Grant No. 20090001120004) and the Scientific Research Foundation for the Returned Overseas Chinese Scholars.

[1] H. Mabuchi and A. C. Doherty, *Science* **298**, 1372 (2002).
[2] G. Khitrova, H. M. Gibbs, M. Kira, S. W. Koch, and A. Scherer, *Nature Phys.* **2**, 81 (2006).
[3] V. B. Braginsky, M. L. Gorodetsky, and V. S. Ilchenko, *Phys. Lett. A* **137**, 393 (1989).
[4] N. Le Thomas *et al.*, *Nano Lett.* **6**, 557 (2006); Y.-S. Park *et al.*, *Nano Lett.* **6**, 2075 (2006); S. Schietinger, T. Schroder, and O. Benson, *Nano Lett.* **8**, 3911 (2008).

[5] E. Peter *et al.*, *Phys. Rev. Lett.* **95**, 067401 (2005); T. Aoki *et al.*, *Nature* **443**, 671 (2006); K. Srinivasan and O. Painter, *Nature* **450**, 862 (2007); K. Srinivasan, C. P. Michael, R. Perahia, and O. Painter, *Phys. Rev. A* **78**, 033839 (2008); J.-T. Shen and S. Fan, *Phys. Rev. A* **79**, 023838 (2009).
[6] T. Gaebel *et al.*, *Nature Physics* **2**, 408 (2006).
[7] F. Jelezko *et al.*, *Phys. Rev. Lett.* **93**, 130501 (2004); R. J.

- Epstein, F. M. Mendoza, Y. K. Kato, D. D. Awschalom, Nat. Phys. **1**, 94 (2005); M. V. Gurudev Dutt *et al.*, Science **316**, 1312 (2007).
- [8] P. E. Barclay, C. Santori, K.-M. Fu, R. G. Beausoleil, and O. Painter, Opt. Express **17**, 8082 (2009).
- [9] E. Waks and J. Vuckovic, Phys. Rev. Lett. **96**, 153601 (2006).
- [10] D. K. Armani, T. J. Kippenberg, S. M. Spillane, and K. J. Vahala, Nature **421**, 925 (2003).
- [11] A. Mazzei *et al.*, Phys. Rev. Lett. **99**, 173603 (2007); J. Zhu *et al.*, Nature Photonics **4**, 46 (2010).
- [12] C. W. Gardiner and P. Zoller, *Quantum Noise*, 3rd ed. Springer, Berlin, 2004.
- [13] B. Dayan *et al.*, Science **319**, 1062 (2008).
- [14] K. Srinivasan and O. Painter, Phys. Rev. A **75**, 023814 (2007).
- [15] H. J. Carmichael, *Statistical Methods in Quantum Optics 2: Non-classical fields*. Springer, Berlin, 2008.
- [16] H. J. Carmichael, Phys. Rev. Lett. **55**, 2790 (1985).
- [17] A. Imamoglu, H. Schmidt, G. Woods and M. Deutsch, Phys. Rev. Lett. **79**, 1467 (1997).
- [18] H. Uys *et al.*, Phys. Rev. Lett. **105**, 200401 (2010).